ORGANOMETALLICS

pubs.acs.org/Organometallics

Article

Well-Defined ENENES Re and Mn Complexes and Their Application in Catalysis: The Role of Potassium *tert*-Butoxide

Liana Ribeiro Gouveia and Elon A. Ison*

Cite This: *Organometallics* 2022, 41, 2678−2687

Read Online

ACCESS | Metrics & More | Article Recommendations | Supporting Information

ABSTRACT: A new family of air-stable Re and Mn complexes bearing bidentate NNS (ENENES) ligands with the general formula $E(CH_2)_2NH(CH)_2SR$ (E = $-NC_4H_8O$ or $-NC_5H_{10}$, R = Ph or thiophenyl) is introduced. All Re and Mn complexes were catalysts for the hydrogenation of aldehydes. The Mn catalysts were active at milder conditions. A rhenium−hydride complex, featuring *cis* Re−H and N−H moieties, was isolated to provide an insight into the mechanism for this reaction. DFT (B3PW91-D3) and experimental data suggest that there are two pathways for this system, with and without the presence of the base (*t*-BuOK). The pathway that included *t*-BuOK was lower in energy, providing a greater driving force for the overall reaction.

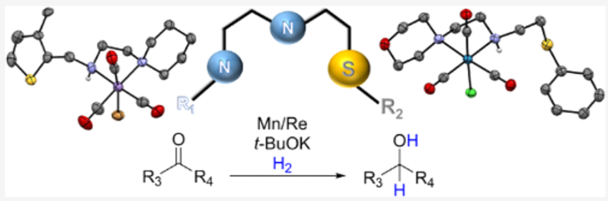

INTRODUCTION

The hydrogenation of carbonyl derivatives is one of the most fundamental and widely employed catalytic reactions.[1] Catalytic methods are more cost-effective and cleaner (minimize waste) compared to methods that employ stoichiometric reducing agents such as lithium aluminum hydride and sodium borohydride.[1] Most metal complexes employed in the catalytic hydrogenation of carbonyl derivatives are based on noble metals such as ruthenium, iridium, and rhodium.[2] Typically, the strategy employed for the activation of substrates involves an oxidative addition/reductive elimination pathway and therefore relies on the availability of stable oxidation states, on the metal center, one or two electrons higher. However, the strategy of metal ligand cooperativity (MLC) has been utilized where both the transition metal and the ancillary ligand participate in the activation of the substrate.[3−17] These strategies allow for the use of catalysts that involve transition metals, where a two-electron redox couple may not be available. Results[1,12,18−20] for the hydrogenation of difficult substrates such as esters and amides are promising for some catalytic systems that employ this strategy. However, it is important to explore other systems with different transition metals.

Transition metal complexes in group 7 such as rhenium and manganese have not been as popular as catalysts for the hydrogenation of carbonyl compounds.[21] However, in the case of manganese, there has been intense research since 2016, and this field has been evolving rapidly with several promising ligand systems.[6,10,22−35] The work in this manuscript was inspired by a report by the Gordon group in 2015 about a new class of NNS ligands (ENENES).[8] In that report, several ENENES ligands and the corresponding ruthenium and iridium complexes were synthesized and used as catalysts for homogeneous hydrogenation of carbonyl compounds (Chart 1a).

Chart 1. Selected Examples of ENENES Complexes (a,b), Mn(I) Precatalysts with a Labile Phosphine Arm (c), and Complexes Used in This Work (d).

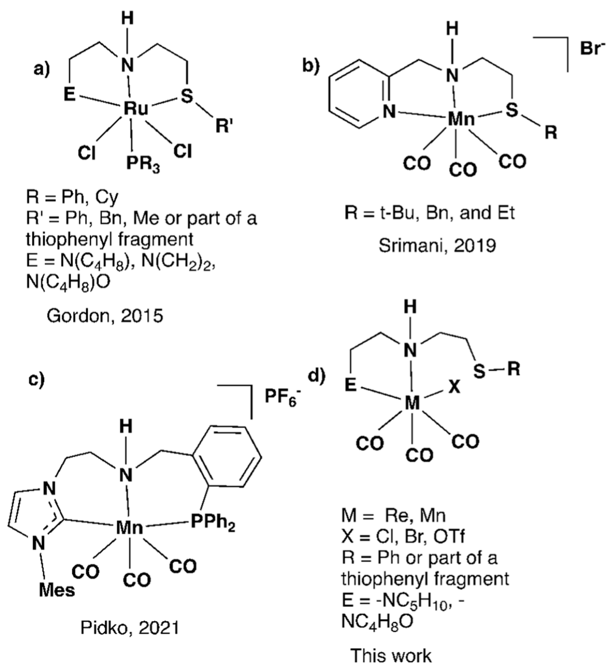

Received: May 28, 2022
Published: September 26, 2022

This report led us to explore the synthesis of ENENES Re and Mn complexes. Unexpectedly, the sulfur arm was not coordinated with the metal center (Chart 1d), unlike a similar series of Mn complexes reported by Srimani (Chart 1b).[36] In the work reported by the Pidko group (Chart 1c),[27] the high activity for the catalytic hydrogenation of carbonyl compounds was proposed to be the result of the very unique phosphine hemilability of the ligand, which results in an unusual pathway for known Mn complexes where the loss of a CO ligand was not needed to form the hydride complex in the active catalyst (Scheme 1). In this article, since the sulfur arm is not coordinated with the metal center, we hypothesized that this feature can also facilitate a similar mechanism since it will very likely not be necessary to lose a CO ligand.

Scheme 1. Synthesis of the Manganese−Hydride Complex Reported by Pidko[27]

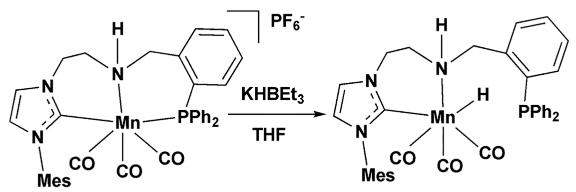

Herein, we introduce a new family of Re and Mn complexes bearing bidentate ENENES ligands of the general formula $E(CH_2)_2NH(CH)_2SR$, where E is either $-NC_4H_8O$ or $-NC_5H_{10}$ and R is Ph or thiophenyl. Reactions of the ENENES ligands with $Re(CO)_5Cl$ and $Mn(CO)_5Br$ are described, along with crystallographic studies of these new complexes. DFT (B3PW91-D3) and experimental data were collected to study the possible mechanism for the hydrogenation of carbonyl compounds. Together, these results provide new insights for pathways for catalytic systems that utilize MLC as a strategy for the activation of small molecules. In addition, the role of potassium *tert*-butoxide, (*t*-BuOK), which is used as an additive in many catalytic systems, has been clarified.

■ RESULTS AND DISCUSSION

Synthesis and Crystallographic Studies of Well-Defined Rhenium and Manganese Complexes of ENENES. The reaction of piperidine and morpholine ENENES derivatives with Re and Mn complexes of the general formula $M(CO)_5X$ (M = Re and Mn; X = Cl and Br) was investigated to examine their reactivity as catalysts for the hydrogenation of carbonyl derivatives. A summary of these reactions is presented in Scheme 2.

Treatment of Re(I) and Mn(I) precursors with the ENENES ligands in benzene at 80 °C (16 h) afforded isostructural $\kappa^2[N,N']$-bidentate *cis*-$[M^IX\{\kappa^2(N,N')\text{-ENENES}\}(CO)_3]$ (M = Re and Mn; X = Cl and Br) complexes **Re-1a** (white solid, isolated yield 92.1%), **Re-1b** (off-white solid, isolated yield 86.5%), **Mn-1a** (yellow solid, isolated yield 41.4%), **Mn-1b** (yellow solid, isolated yield 68.3%), and **2** (off-white solid, isolated yield 90.4%), respectively. Complexes **Re-1a**, **Re-1b**, **Mn-1a**, **Mn-1b**, and **2** are air stable and are characterized by NMR (^1H, ^{13}C) spectroscopy, elemental analysis, and X-ray structural analysis.

X-ray quality crystal structures were obtained by vapor diffusion of hexane into concentrated solutions of **Re-1a**, **Mn-1a**, and **2** in chloroform. The crystal structures (Figure 1 and Supporting Information) of these complexes closely resemble each other—the sulfur arm is not coordinated with the metal center, and the three carbonyl groups are *cis* to each other, featuring a *facial (fac)* arrangement of the CO ligands with an octahedral metal center.

Scheme 2. Reaction of ENENES Ligands with $M(CO)_5X$ (M = Re and Mn; X = Cl and Br) to Produce Precatalysts for Hydrogenation of Carbonyl Derivatives

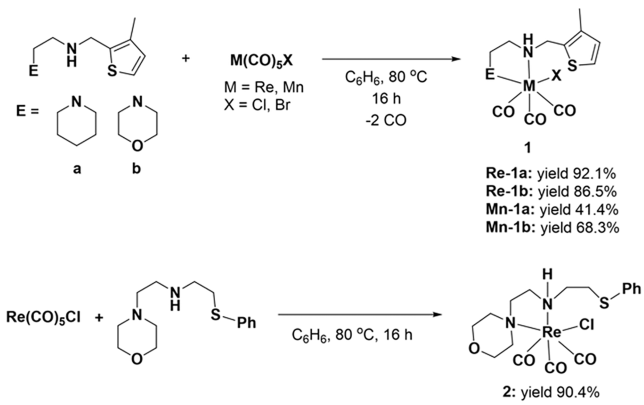

Thermal Stability of the ENENES Complexes. Decomposition tests were performed on the new ENENES complexes. These tests consisted of heating NMR samples in oil baths at temperatures 40, 60, 80, 100, and 120 °C for 16 h. As shown in Figure 2, **Re-1b** did not decompose at 120 °C.

Both manganese complexes decomposed at 40 °C, which suggests that any catalysis with these complexes would have to be performed at lower temperatures (40 °C or below) (Chart 2). Like **Re-1b**, **Re-1a** and **2** did not decompose at 120 °C (Chart 2).

Hydrogenation Activity of the ENENES Complexes. The catalytic hydrogenation of benzaldehyde with the ENENES complexes was examined in THF to find the most active catalyst and the optimal conditions for the hydrogenation reaction. The results presented in Table 1 indicate that the complex **Mn-1b** performed the hydrogenation of benzaldehyde at 50 bar of H_2 more efficiently than the other ENENES complexes investigated (entry 4).

Catalyst **Re-1b** had similar results; however, it required a slightly higher temperature than 25 °C (entry 2). High yields were also observed when the pressure of H_2 was decreased to 40 bar (entry 5); however, yields decreased significantly when the pressure was decreased to 30 and 20 bar (entries 6 and 7, respectively). Other solvents such as acetonitrile, diethyl ether, and 1,4-dioxane were tested with catalyst **Mn-1b**, but they did not perform, as well as THF (Supporting Information). The base potassium *tert*-butoxide, *t*-BuOK, was necessary as a cocatalyst. Reactions with 10 equiv of *t*-BuOK (entry 5) were more efficient than reactions performed with 2 (entry 8) and 5 (entry 9) equiv, respectively, with respect to **Mn-1b**. Thus, entry 5 represents the optimal conditions for the hydrogenation reactions with **Mn-1b**, that is, 0.5 **Mn-1B**, 5 mol % *t*-BuOK at 40 bar H_2 pressure and 25 °C.

Mechanistic Investigation. In catalysis, complexes that have functional groups in the ligand that assist in the activation of the substrates are typically referred to as bifunctional catalysts.[36] With these catalysts, the usual approach to activate the precatalyst is to use an excess of a strong base such as *t*-BuOK, followed by the addition of H_2 at high pressure to form a catalytically active metal hydride intermediate, in

https://doi.org/10.1021/acs.organomet.2c00261
Organometallics 2022, 41, 2678−2687

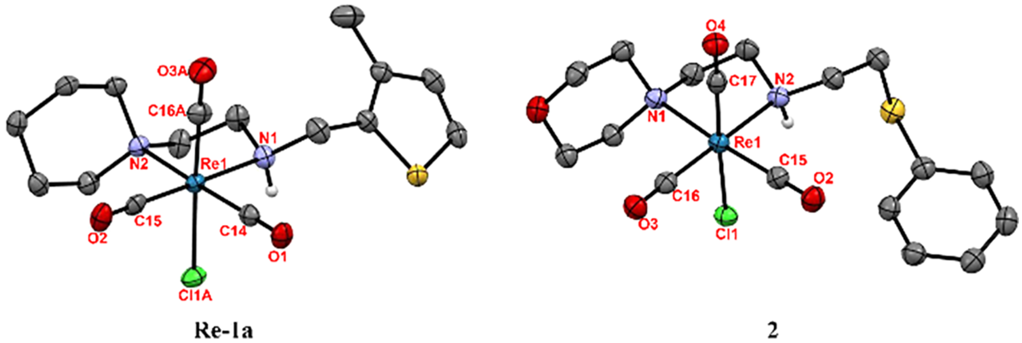

Figure 1. X-ray structures for Re complexes **Re-1a** and **2**. Ellipsoids are at 50% probability level. Hydrogen atoms (except NH) are omitted for clarity. Selected bond lengths (Å) and angles (°) for **Re-1a**: Re1−Cl1, 2.497(6); Re1−N1, 2.239(3); Re1−N2, 2.309(3); Re1−C14, 1.910(4); Re1−C15, 1.921(4); Re1−C16A, 1.856(14); O1−C14, 1.152(5); O2−C15, 1.143(5); O3A−C16A, 1.161(15); C16A−Re1−C14, 89.2(5); C16A−Re1−C15, 89.0(5); C14−Re1−C15, 87.09(16); C16A−Re1−N1, 93.8(3); C15−Re1−N1, 179.11(15); C16A−Re1−N2, 95.3(2); C15−Re1−N2, 99.67(14); C16−Re1−Cl1A, 177.5(2); C15−Re1−Cl1A, 94.36(14); N2−Re1−Cl1A, 87.14(10); C14−Re1−Cl1A, 91.21(17); and N1−Re1−Cl1A, 85.41(15). Selected bond lengths (Å) and angles (°) for **2**: Re1−Cl1, 2.4736(7); Re1−N1, 2.316(3); Re1−N2, 2.224(3); Re1−C15, 1.918(3); Re1−C16, 1.913(3); Re1−C17, 1.901(3); O2−C15, 1.150(4); O3−C16, 1.157(4); O4−C17, 1.161(4); C17−Re1−C15, 89.09(13); C16−Re1−C17, 88.46(13); C15−Re1−C16, 86.72(13); N2−Re1−C17, 93.16(12); N2−Re1−C16, 177.90(11); N1−Re1−C17, 93.22(11); N1−Re1−C16, 99.50(11); Cl1−Re1−C17, 174.60(9); Cl1−Re1−C16, 96.79(9); Cl1−Re1−N1, 84.68(7); Cl1−Re1−C15, 92.46(10); and Cl1−Re1−N2, 81.56(7).

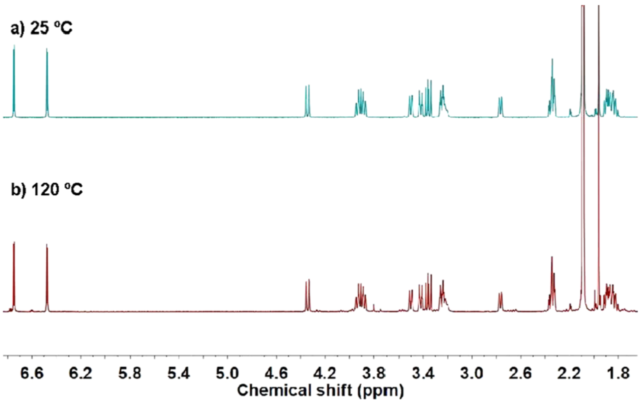

Figure 2. ^{1}H NMR spectra of **Re-1b** in toluene-d_8 at (a) 25 and (b) 120 °C.

Chart 2. Thermal Stability of the ENENES Complexes after 16 h.

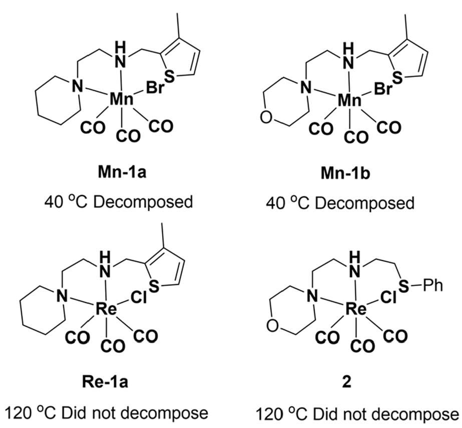

Table 1. Hydrogenation of Benzaldehyde with Several Rhenium and Manganese Catalysts

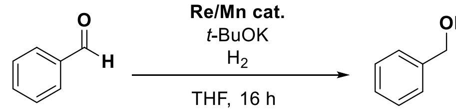

entry	catalyst	cat. loading (mol %)	additive (mol %)	pressure (bar)	temp. (°C)	yield (%)
1	**Re-1a**	0.5	5	50	40	87
2	**Re-1b**	0.5	5	50	40	95
3	**Mn-1a**	0.5	5	50	25	81
4	**Mn-1b**	0.5	5	50	25	95
5	**Mn-1b**	0.5	5	40	25	95
6	**Mn-1b**	0.5	5	30	25	80
7	**Mn-1b**	0.5	5	20	25	24
8	**Mn-1b**	0.5	1	40	25	ND[a]
9	**Mn-1b**	0.5	2.5	40	25	20
10	**Re-1b**	0.5	5	50	25	57
11	**2**	0.5	5	50	50	66
12	**Re-1b**	0.5	5	50	50	>99
13[b]	**Re-1b**	0.1	1	50	100	16
14	—	—	5	50	40	14

[a]ND = not detected. [b]Reaction was conducted in toluene.

Scheme 3. Synthesis of 3 from Re-1b

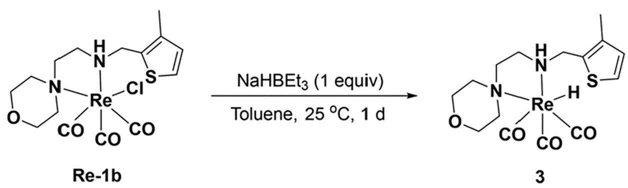

situ.[1,5,10,25,27−30,32,33,37−43] This hydride intermediate would then transfer hydrogens to the substrate.

The rhenium complex **3** (Scheme 3) was successfully synthesized in 78.4% yield. The crystal structure for **3** is shown in Figure 3 and demonstrates that the chloride ligand has been replaced by the hydride ligand, and the facial arrangement of the carbonyl ligands has been maintained.

The HReNH core of this complex resembles others that have been used as bifunctional catalysts previously in the literature, such as those reported by Choualeb et al.[44] and the Sortais group.[45] The latter complex contrasts with **3** since the hydride in

https://doi.org/10.1021/acs.organomet.2c00261
Organometallics 2022, 41, 2678−2687

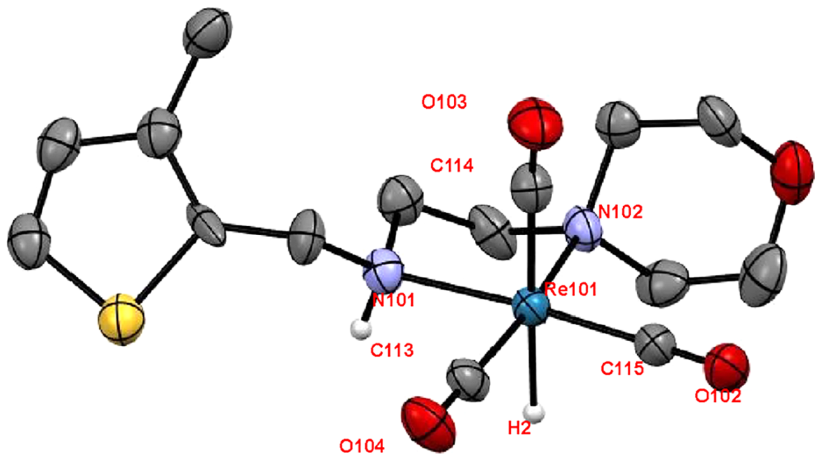

Figure 3. X-ray structure for **3**. Ellipsoids are at 50% probability level. Hydrogen atoms (except NH and ReH) are omitted for clarity. Selected bond lengths (Å) and angles (°): Re101−H2, 1.746(10); Re101−N101, 2.238(6); Re101−N102, 2.293(7); Re101−C113, 1.899(8); Re101−C114, 1.949(6); Re101−C115, 1.922(8); O102−C115, 1.147(10); O103−C114, 1.147(8); O104−C113, 1.174(10); C113−Re101−C114, 89.7(3); C113−Re1−C115, 86.4(3); C114−Re1−C115, 88.2(3); N101−Re101−N102, 79.5(2); N101−Re101−C113, 91.7(3); N102−Re101−C113, 169.4(3); N101−Re101−C114, 94.4(3); N102−Re101−C114, 96.8(3); N101−Re101−C115, 176.7(3); N102−−Re101−C115, 102.1(3); N101−Re101−H2, 86.6(16); N102−Re101−H2, 83(3); C113−Re101−H2, 91(3); C114−Re101−H2, 178.74(10); and C115−Re101−H2, 90.7(17).

the Re−H bond and the proton in the N−H bond are *anti* to each other and is most likely not the active catalyst.[45]

To test the participation of **3** in the reaction, the stoichiometric reaction of **3** with benzaldehyde was performed. The addition of 1 equiv of benzaldehyde to **3** readily formed the new rhenium species **4** (Scheme 4). Complex **4** could not be isolated, but the ^{1}H NMR spectrum (Figure 4) exhibited two doublets in the characteristic region for a methylene group that has the two protons in different chemical environments, suggesting that it is most likely an alkoxide complex.

Scheme 4. Reaction of 3 with 1 equiv of Benzaldehyde in Toluene-d_8

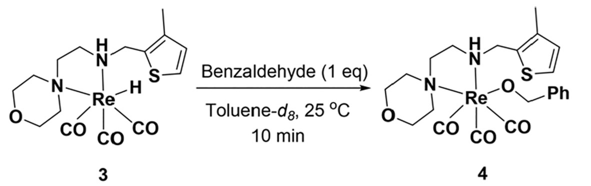

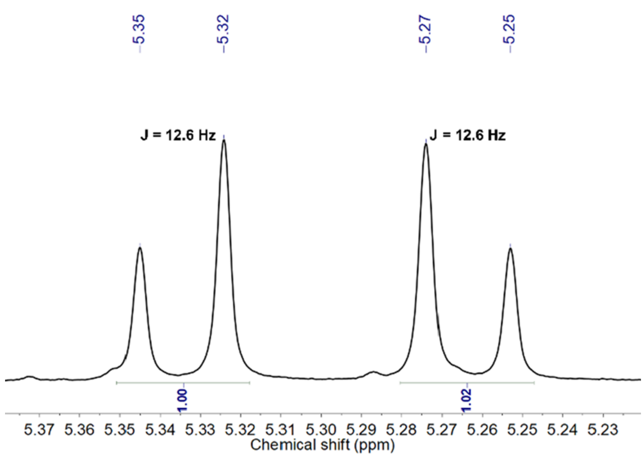

Figure 4. ^{1}H NMR spectrum of the methylene region of **4**.

This piece of evidence along with COSY, HSQC, and HMBC spectra (Supporting Information) helped us to tentatively assign **4** as illustrated in Scheme 4.

When complex **3** was used as a catalyst for the hydrogenation reaction of benzaldehyde without the additive, *t*-BuOK catalysis was poor (Figure 5). However, in the presence of *t*-BuOK, yields significantly improved.

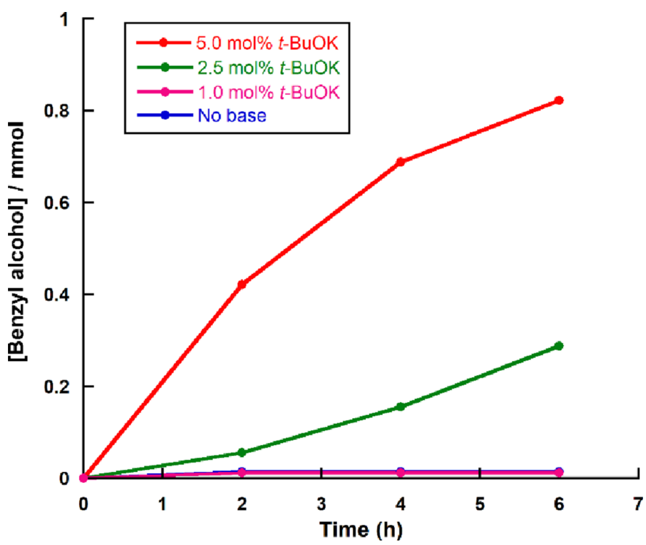

Figure 5. Time profile for hydrogenation of benzaldehyde. Conditions: [**3**] = 0.0045 mmol; [*t*-BuOK] = 0.0045 mmol (1.0 mol %), 0.0225 mmol (2.5 mol %), and 0.045 mmol (5.0 mol %); [benzaldehyde] = 0.9 mmol at 25 °C. H_2 pressure = 50 bar. Conversions determined by ^{1}H NMR spectroscopy by integrating the ratio of the methylene peak in the alcohol product and the aldehyde peak of the substrate.

This finding suggests that *t*-BuOK is part of the catalytic cycle. To test this hypothesis, we ran two experiments: (1) the catalytic hydrogenation of benzaldehyde with **Re-1b** using only 1 equiv of *t*-BuOK in relation to rhenium and (2) the stoichiometric reaction of **3** with benzaldehyde in the presence of a stoichiometric amount of *t*-BuOK. Experiment 1 (Figure 6) revealed that without an excess amount of *t*-BuOK,

https://doi.org/10.1021/acs.organomet.2c00261
Organometallics 2022, 41, 2678−2687

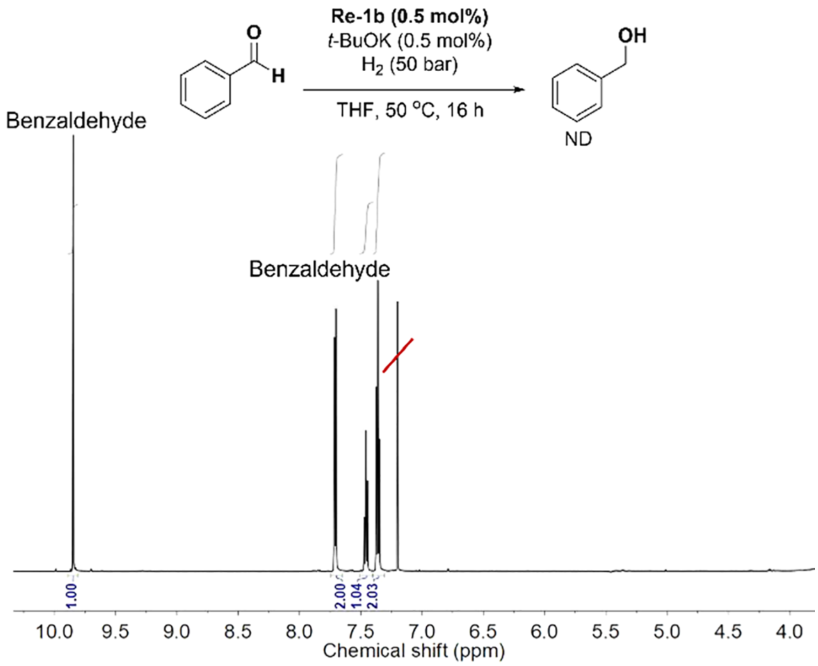

Figure 6. ^{1}H NMR spectrum of the catalytic hydrogenation of benzaldehyde with **Re-1b** and 1 equiv of *t*-BuOK.

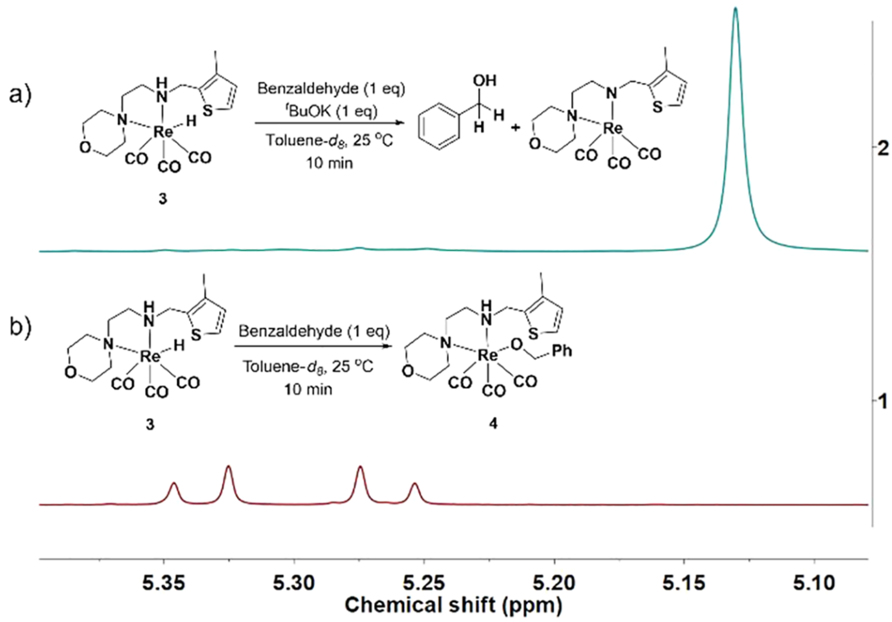

Figure 7. ^{1}H NMR spectra of the stoichiometric reactions of **3** with benzaldehyde with (a) and without (b) *t*-BuOK.

benzaldehyde could not be converted to benzyl alcohol. A similar experiment was performed with the analogous Mn complex, which behaved as the Re complex **Re-1b**.

The stoichiometric reaction (experiment 2, Figure 7) resulted in a singlet in the ^{1}H NMR spectrum in the methylene region, characteristic of benzyl alcohol. This contrasts with the stoichiometric reaction in the absence of *t*-BuOK (Scheme 4). Together, these two experiments show that the base *t*-BuOK is a part of the catalytic cycle. Specifically, results suggest that *t*-BuOK assists in the release of the product benzyl alcohol since the stoichiometric reaction of **3** with benzaldehyde in the absence of base led to the formation of **4**.

Based on our experimental results, we propose a possible reaction mechanism for the homogeneous hydrogenation of aldehydes catalyzed by the ENENES complexes of rhenium and manganese introduced in this study. The ligand backbone in the precatalyst, in the presence of the base *t*-BuOK, is likely deprotonated to form **A** (Scheme 5).

Once formed in situ, **A** splits dihydrogen heterolytically by metal ligand cooperativity (MLC), generating the hydride complex **B**. Two pathways are proposed for the reaction of **B** with the carbonyl substrate. In path I, the introduction of benzaldehyde forms the alkoxide complex **C**, which then will go through a transition state to transfer the proton from the N−H bond to the nucleophilic oxygen of benzaldehyde. The dissociation of the product regenerates **A**.

https://doi.org/10.1021/acs.organomet.2c00261
Organometallics 2022, 41, 2678−2687

Scheme 5. Proposed Reaction Mechanism for the ENENES Re-Catalyzed Hydrogenation of Aldehydes to Alcohols[a]

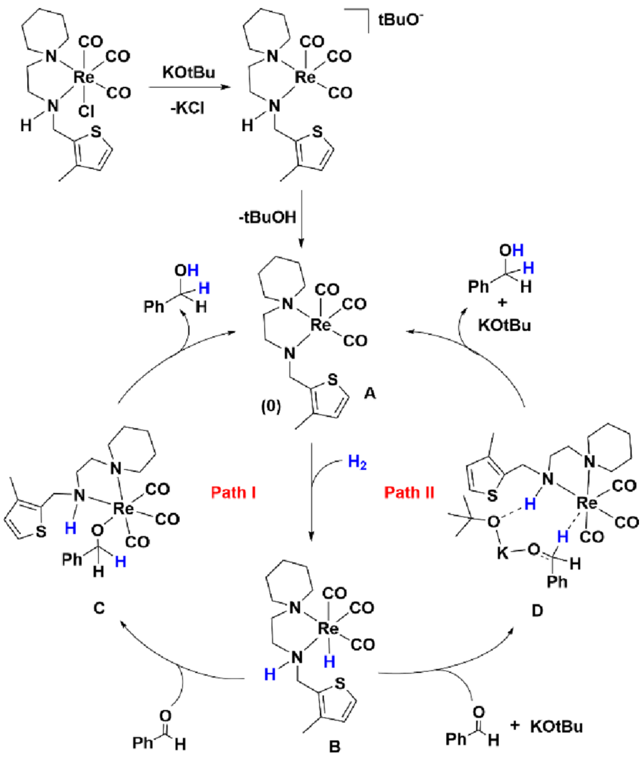

[a]Energies from DFT (B3PW91-D3) calculations are reported in kcal/mol; the nitrogen moiety indicates that it can either be morpholine or piperidine.

In path II, *t*-BuOK initially interacts with benzaldehyde to form an adduct that reacts with **B** to form **D**. The product is released from **D** to regenerate **A** and *t*-BuOK.

DFT Calculations. To examine these pathways, we employed DFT (B3PW91-D3) calculations. Figure 8 shows the calculated pathways for **Re-1a**. The calculated free energy pathway is consistent with the experimental results and shows that **TS1**, that is, the heterolytic splitting of the dihydrogen molecule, is the turnover limiting step (24.7 kcal/mol). This step produces **B** which then reacts with benzaldehyde to generate the desired product, benzyl alcohol, and regenerate the active catalyst (**Int-5**) via **TS2** (4.7 kcal/mol) and **TS4** (−3.7 kcal/mol).

In path II, **B** interacts with an adduct of benzaldehyde and *t*-BuOK to generate **Int-2**. This intermediate goes through a transition state **TS3** (2.2 kcal/mol) to form **D**, which will then have the hydride on the metal center transferred to the electrophilic carbon on benzaldehyde (**Int-4**). The following transition state **TS5** (−5.1 kcal/mol) leads to the desired product benzyl alcohol with the regeneration of the active catalyst (**Int-6**).

The two major differences in the two pathways are the driving force for the overall reaction and the activation barrier necessary to release the product. In path II, the overall reaction is significantly more downhill (−34.6 kcal/mol) than path I (−5.0 kcal/mol), and the activation barrier for product release for pathway I is 14.7 kcal/mol while for pathway II is 1.6 kcal/mol. Thus, it appears that *t*-BuOK assists in the release of the organic product benzyl alcohol. DFT structures (see the Supporting Information) suggest that the thiophene ring interacts weakly with potassium atom on *t*-BuOK and allows this additive to remain in the metal coordination sphere.

Substrate Scope. Finally, the optimal conditions (entry 5, Table 1) were selected to examine the versatility of our system. As shown in Table 2, entries **5a**−**5e** high yields were achieved under these conditions, showing that this system is selective toward aliphatic aldehydes and aromatic aldehydes with electron-withdrawing groups in the para position. Moderate yields were obtained for **5f**, despite the potential for this substrate to bind κ^2 to the metal center. Low yields were

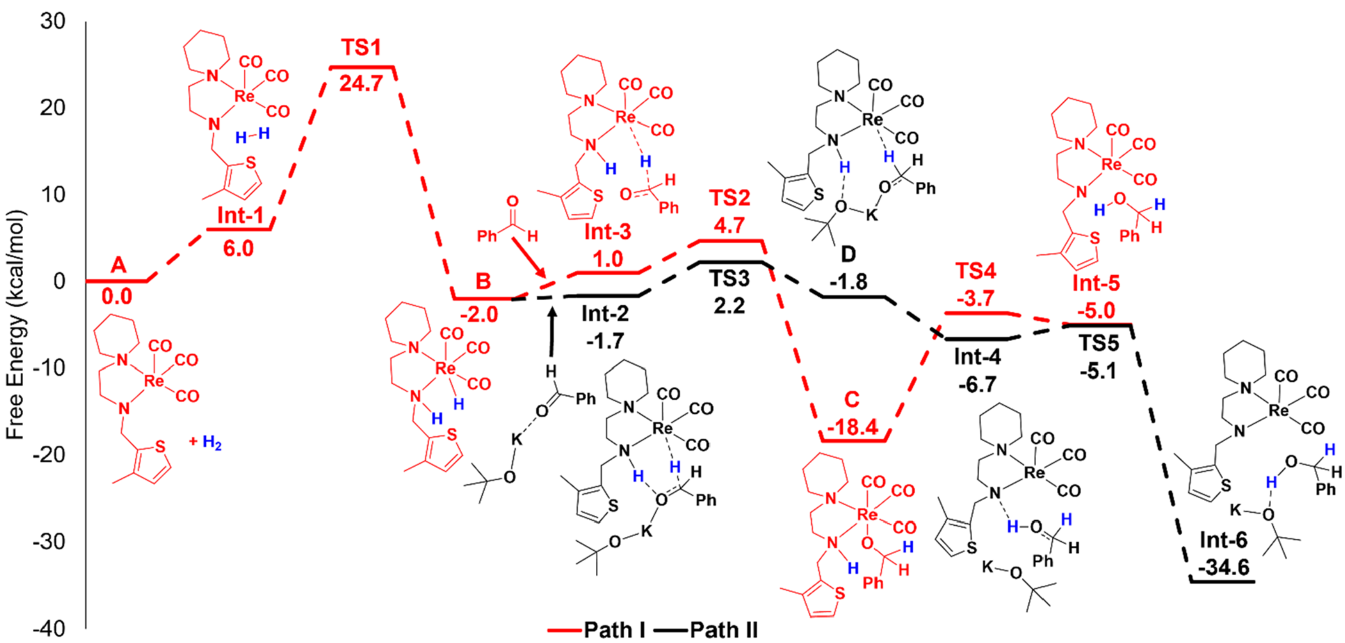

Figure 8. Calculated (B3PW91-D3) free energy pathways for the hydrogenation of benzaldehyde catalyzed by **Re-1a** with (black) and without (red) *t*-BuOK. Solvation energies are reported using the PCM solvation model in toluene.

https://doi.org/10.1021/acs.organomet.2c00261
Organometallics 2022, 41, 2678−2687

Table 2. Hydrogenation of Aldehydes 5a to 5i with Catalyst Mn-1b[a]

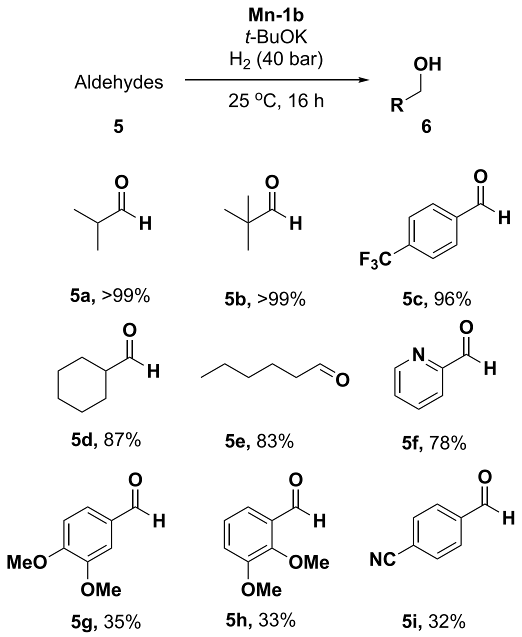

[a]Yields are in triplicate and calculated by ^{1}H NMR spectroscopy. For complexes **5d** and **5e**, % conversion is reported.

observed for substrates with weak electron-withdrawing groups on an aryl aldehyde. A competition experiment was also performed where aldehyde and acetophenone were present in the same reaction vessel. Under these conditions, acetophenone was not hydrogenated, suggesting that this system is selective for aldehydes over ketones.

■ CONCLUSIONS

In summary, several ENENES Mn(I) and Re(I) complexes were prepared and tested as catalysts for the homogeneous hydrogenation of benzaldehyde. Although all the complexes were able to hydrogenate the aldehydes, the manganese complex **Mn-1b** was found to be the most efficient catalyst for this system under mild conditions, that is, 25 °C and 40 bar H_2 pressure. The isolation of the rhenium-hydride complex **3** made it possible to study the mechanism, and it was experimentally observed that the base *t*-BuOK is an important part of the catalytic cycle, where it most likely assists in the release of the desired product. Based on experimental and computational studies, two pathways have been proposed for this system: with and without the presence of the base (*t*-BuOK). The path that included *t*-BuOK was lower in energy. To the best of our knowledge, the rhenium complexes reported here are the first ones bearing ENENES ligands. Further, this is also the first study where the role of *t*-BuOK, which is frequently used as an additive in many catalytic systems, is clarified. Given the ubiquity of this additive in many catalytic systems, we believe that this work will be of interest to many in the community.

■ EXPERIMENTAL SECTION

General Considerations. Complexes $Re(CO)_5Cl$ and $Mn(CO)_5Br$ and ligand **2′** were purchased from Strem Chemicals and used as received. Ligands a and b were synthesized according to the published procedures.[8] Anhydrous solvents were purchased from Sigma-Aldrich and dried with molecular sieves before use. Potassium *tert*-butoxide (1.0 M in THF) and sodium triethylborohydride (1.0 M in toluene) were purchased from Sigma-Aldrich and used as received. Aldehydes were purchased from Sigma-Aldrich and Fisher Scientific: solids were used as received, and the liquids were dried with molecular sieves and degassed before use. Air- and/or moisture-sensitive materials were stored in the glovebox. Deuterated solvents were purchased from Cambridge Isotope Laboratories. ^{1}H and ^{13}C NMR spectra were obtained on 500 or 600 MHz spectrometers at room temperature. Chemical shifts are listed in parts per million (ppm) and referenced to the residual protons of the deuterated solvent used. Elemental analyses were performed by Atlantic MicroLabs, Inc. X-ray crystallography was performed by Jenny S. Forester, Roger D. Sommer, and Chun-Hsing Chen (UNC Chapel Hill Chemistry) at the Molecular Education, Technology and Research Innovation Center (METRIC) at NC State University.

Synthesis of Re(NNS(thiophene)-piperidine)(Cl)(CO)$_3$ (Re-1a). Ligand **a** (299 mg, 1.26 mmol) was dissolved in 20 mL of dry benzene and was added dropwise to a colorless suspension of [$Re(CO)_5Cl$] (454 mg, 1.26 mmol) and 40 mL of dry benzene. The mixture was then refluxed overnight under a nitrogen atmosphere in a 100 mL Schlenk flask. After cooling to room temperature, the solvent was evaporated, and the residue was further stirred with hexanes overnight, filtered, and dried under vacuum to yield a white solid of the Re complex **Re-1a**. Yield: 92.1%, 1.4 g. A single crystal was grown by slow diffusion of hexanes in a chloroform solution of the complex at room temperature. ^{1}H NMR (600 MHz, $CDCl_3$): δ 7.21 (d, J = 5.1 Hz, 1H, thiophene-*H*), 6.87 (d, J = 5.1 Hz, 1H, thiophene-*H*), 4.76−4.68 (m, 1H, NH−C*H*$_2$-thiophene), 4.08−3.99 (m, 1H, NH−C*H*$_2$-thiophene), 3.71−3.64 (m, 1H, −C*H*$_2$−), 3.61−3.53 (m, 1H, −C*H*$_2$−), 3.43 (s, 1H, N*H*), 3.21−3.15 (m, 1H, −C*H*$_2$−), 2.99−2.92 (m, 1H, −C*H*$_2$−), 2.77−2.68 (m, 2H, piperidine), 2.61−2.53 (m, 2H, piperidine), 2.28 (s, 3H, C*H*$_3$-thiophene), 2.00−1.91 (m, 2H, piperidine), 1.84−1.77 (m, 2H, piperidine), 1.66−1.60 (m, 1H, piperidine), 1.49−1.43 (m, 1H, piperidine). ^{13}C NMR (151 MHz, $CDCl_3$): δ 196.58193.82, 192.92, 137.56, 131.53, 130.92, 125.08, 63.25, 59.39, 53.42, 48.94, 31.80, 24.06, 23.67, 23.21, 14.17. FTIR cm^{-1}: 2015, 1871, and 1845 (Re-CO). Elemental analysis: ($C_{16}H_{22}ClN_2O_3ReS$) Theory: (C, 35.30; H, 4.04; N, 5.15) Found: (C, 35.05; H, 4.04; N, 5.13).

Synthesis of Re(NNS(thiophene)-morpholine)(Cl)(CO)$_3$ (Re-1b). Ligand **b** (415 mg, 1.73 mmol) was dissolved in 20 mL of dry benzene and was added dropwise to a colorless suspension of [$Re(CO)_5Cl$] (626 mg, 1.73 mmol) and 40 mL of dry benzene. The mixture was then refluxed overnight under a nitrogen atmosphere in a 100 mL Schlenk flask. After cooling to room temperature, the solvent was evaporated, and the residue was further stirred with hexanes overnight, filtered, and dried under vacuum to yield a light purple solid of Re complex **Re-1b**. Yield: 86.5%, 817 mg. A single crystal was grown by slow diffusion of hexanes in a chloroform solution of the complex at room temperature. ^{1}H NMR (600 MHz, CD_2Cl_2): δ 7.28 (d, J = 5.1 Hz, 1H, thiophene-*H*), 6.92 (d, J = 5.1 Hz, 1H, thiophene-*H*), 4.74−4.68 (m, 1H, NH−C*H*$_2$-thiophene), 4.14−4.08 (m, 2H, morpholine), 4.07−4.02 (m, 1H, NH−C*H*$_2$-thiophene), 4.01−3.97 (m, 1H, −C*H*$_2$−), 3.84−3.79 (m, 1H, −C*H*$_2$−), 3.78−3.74 (m, 1H, −C*H*$_2$−), 3.57−3.52 (m, 1H, −C*H*$_2$−), 3.47 (s, 1H, N*H*), 3.26−3.21 (m, 1H, morpholine), 3.16−3.10 (m, 1H, morpholine), 2.93−2.87 (m, 1H, morpholine), 2.82−2.74 (m, 1H, morpholine), 2.66−2.59 (m, 2H, morpholine), 2.30 (s, 3H, C*H*$_3$-thiophene). ^{13}C NMR (126 MHz, $CDCl_3$): δ 196.21, 193.43, 192.72, 137.88, 131.47, 131.19, 125.45, 65.41, 65.31, 62.99, 62.16, 57.92, 53.76, 48.42, 14.38. FTIR cm^{-1}: 2016, 1895, and 1880 (Re-CO). Elemental analysis: ($C_{15}H_{20}ClN_2O_4ReS\cdot 0.5CH_2Cl_2$) Theory: (C, 31.63; H, 3.60; N, 4.76) Found: (C, 31.71; H, 3.47; N, 4.65).

Synthesis of Mn(NNS(thiophene)-piperidine)(Br)(CO)$_3$ (Mn-1a). Ligand **a** (266 mg, 1.12 mmol) was dissolved in 20 mL of dry benzene and was added dropwise to a colorless suspension of [$Mn(CO)_5Br$] (307 mg, 1.12 mmol) and 40 mL of dry benzene. The mixture was then refluxed overnight under a nitrogen atmosphere in a 100 mL Schlenk flask. After cooling to room temperature, the solvent was evaporated, and the residue was further stirred with hexanes overnight, filtered, and dried under vacuum to yield a light-yellow solid

https://doi.org/10.1021/acs.organomet.2c00261
Organometallics 2022, 41, 2678−2687

of the Mn complex **Mn-1a**. Yield: 41.4%, 212 mg. A single crystal was grown by slow diffusion of hexanes in a chloroform solution of the complex at room temperature. ^{1}H NMR (600 MHz, $CDCl_3$): δ 7.20 (d, J = 5.1 Hz, 1H, thiophene-H), 6.87 (d, J = 5.1 Hz, 1H, thiophene-H), 4.73 (d, 1H, J = 15.0 Hz, NH−CH_2-thiophene), 3.97−3.90 (m, 1H, NH−CH_2-thiophene), 3.60 (broad s, 1H, NH), 3.46 (broad s, 2H, −CH_2−), 3.18 (broad s, 1H, −CH_2−), 3.05−2.98 (m, 2H, piperidine), 2.72−2.54 (m, 4H, piperidine), 2.31 (s, 3H, CH_3-thiophene), 1.82 (m, 1H, −CH_2−), 1.76 (broad s, 2H, piperidine), 1.59 (m, 2H, piperidine). ^{13}C NMR (151 MHz, $CDCl_3$): δ 137.25, 131.50, 130.93, 124.66, 60.76, 60.13, 52.10, 48.29, 28.40, 23.53, 22.48, 22.41, 14.18. Some carbon peaks are lost in the baseline. FTIR cm^{-1}: 2013, 1923, and 1892 (Re-CO). Elemental analysis: ($C_{16}H_{22}BrMnN_2O_3S\cdot0.33CH_2Cl_2$) Theory: (C, 40.32; H, 4.90; N, 5.76) Found: (C, 40.35; H, 4.86; N, 5.99).

Synthesis of Mn(NNS(thiophene)-morpholine)(Br)(CO)$_3$ (Mn-1b). Ligand **b** (314 mg, 1.31 mmol) was dissolved in 20 mL of dry benzene and was added dropwise to a colorless suspension of [Mn(CO)$_5$Br] (360 mg, 1.31 mmol) and 40 mL of dry benzene. The mixture was then refluxed overnight under a nitrogen atmosphere in a 100 mL Schlenk flask. After cooling to room temperature, the crude yellow product precipitated, which was then filtered and washed with hexanes overnight, filtered again, and dried under vacuum to yield a yellow solid of the Mn complex **Mn-1b**. Yield: 68.3%, 411 mg. A single crystal was grown by slow diffusion of hexanes in a chloroform solution of the complex. ^{1}H NMR (600 MHz, $CDCl_3$) δ: 7.21 (s overlapping with the solvent, 1H, thiophene-H), 6.88 (s, 1H, thiophene-H), 4.71 (d, J = 14.98 Hz, 1H, −CH_2−), 4.06−3.89 (m, 4H, morpholine), 3.80−3.69 (m, 2H, −CH_2−), 3.67−3.53 (m, 2H, −CH_2−), 3.03 (broad s, 1H, NH), 2.97−2.87 (m, 2H, morpholine), 2.86−2.79 (m, 1H, −CH_2−), 2.72−2.66 (m, 1H, morpholine), 2.65−2.58 (m, 1H, morpholine), 2.31 (s, 3H, CH_3-thiophene). ^{13}C NMR (151 MHz, $CDCl_3$): δ 137.37, 131.25, 130.98, 124.84, 64.12, 63.37, 60.70, 58.71, 57.06, 52.20, 47.61, 14.18. FTIR cm^{-1}: 2013, 1923, and 1893 (Re-CO). Elemental analysis: ($C_{15}H_{20}BrMnN_2O_4S\cdot0.5CH_2Cl_2$) Theory: (C, 37.11; H, 4.22; N, 5.58) Found: (C, 36.75; H, 4.29; N, 5.79).

Synthesis of Re(NNS(phenyl)-morpholine)(Cl)(CO)$_3$ (2). Ligand **2′** (100 mg, 0.380 mmol) was dissolved in 20 mL of dry benzene and was added dropwise to a colorless suspension of [Re(CO)$_5$Cl] (136 mg, 0.380 mmol) and 40 mL of dry benzene. The mixture was then refluxed overnight under a nitrogen atmosphere in a 100 mL Schlenk flask. After cooling to room temperature, the solvent was evaporated, and the residue was further stirred with hexanes overnight, filtered, and dried under vacuum to yield an off-white solid of Re complex **2**. A single crystal was grown by slow diffusion of hexanes in a chloroform solution of the complex. Yield: 90.4%, 194 mg. ^{1}H NMR (500 MHz, $CDCl_3$): δ 7.55−7.51 (m, 2H, phenyl), 7.38−7.33 (m, 2H, phenyl), 7.33−7.30 (m, 1H, phenyl), 4.16 (s, 1H, NH), 4.14−4.07 (m, 2H, morpholine), 3.98−3.93 (m, 1H, morpholine), 3.87−3.80 (m, 2H, −CH_2−), 3.50−3.44 (m, 1H, morpholine), 3.36−3.33 (m, 1H, −CH_2−), 3.32−3.26 (m, 1H, −CH_2−), 3.25−3.20 (m, 1H, −CH_2−), 3.13−3.08 (m, 1H, −CH_2−), 3.07−3.04 (m, 2H, −CH_2−), 2.85−2.80 (m, 1H, morpholine), 2.68−2.62 (m, 1H, morpholine), 2.61−2.55 (m, 2H, morpholine). ^{13}C NMR (126 MHz, $CDCl_3$): δ 195.91, 193.07, 192.39, 133.25, 131.86, 129.88, 128.68, 65.23, 65.07, 62.68, 61.89, 57.73, 54.85, 47.80, 34.20. FTIR cm^{-1}: 2013, 1914, and 1882 (Re-CO). Elemental analysis: ($C_{17}H_{22}ClN_2O_4ReS$) Theory: (C, 35.66; H, 3.85; N, 4.89) Found: (C, 35.68; H, 3.83; N, 4.89).

Synthesis of Re(NNS(thiophene)-morpholine)(H)(CO)$_3$ (3). In an inert atmosphere, complex **Re-1b** (102.2 mg, 0.187 mmol) was dissolved in 30 mL of dry toluene in a 50 mL storage tube. One equivalent of sodium triethylborohydride (0.187 mL, 0.187 mmol) was added dropwise to the solution of 1bc and stirred overnight (16 h) at room temperature. The solution was then filtered to afford a yellow solid, which consisted of a mixture of the desired product (rhenium−hydride complex **3**) and the byproduct sodium chloride. To separate both products, the yellow powder was dissolved in a minimal amount of methylene chloride and filtered through Celite, and excess pentane was added to afford the precipitation of the desired white Re complex product **3**. Yield: 78.4%, 75.0 mg. A single crystal was grown by slow diffusion of pentane in a methylene chloride solution of the complex. ^{1}H NMR (600 MHz, CD_2Cl_2): δ 7.27 (d, J = 5.2 Hz, 1H, thiophene-H), 6.90 (d, J = 5.1 Hz, 1H, thiophene-H), 4.57 (m, 1H, NH−CH_2-thiophene), 4.43 (s, 1H, NH), 4.12 (m, 2H, morpholine), 3.99 (m, 1H, NH−CH_2-thiophene), 3.94 (dt, J = 12.7, 3.2 Hz, 1H, morpholine), 3.81 (dt, J = 12.9, 3.4 Hz, 1H, morpholine), 3.45 (m, 2H, −CH_2−), 3.22−3.16 (m, 1H, −CH_2−), 2.96−2.89 (m, 3H, overlap between −CH_2− and morpholine), 2.82 (ddd, J = 11.9, 10.2, 3.2 Hz, 1H, morpholine), 2.69 (dtd, J = 13.2, 9.7, 3.6 Hz, 1H, morpholine), 2.28 (s, 3H, CH_3-thiophene), 1.90 (s, 1H, Re−H). ^{13}C NMR (126 MHz, $CDCl_3$): d 201.89, 200.30, 198.20, 137.99, 132.99, 131.12, 125.44, 66.49, 65.82, 64.30, 55.79, 48.12, 14.35. FTIR cm^{-1}: 2016 (Re−H), 1987, and broad peak at 1852 (Re−CO). Elemental analysis: ($C_{15}H_{21}N_2O_4ReS\cdot0.5CH_2Cl_2$) Theory: (C, 33.60; H, 4.00; N, 5.06) Found: (C, 33.76; H, 3.98; N, 5.05).

Computational Studies. Calculations were performed with the Gaussian 16[46] computational program. Geometry and transition-state optimizations were performed with the 6-31G(d,p)[47,48] basis set on light atoms and SDD basis set[49−51] with an added f polarization function[52] on rhenium and manganese. The optimization calculations included tight optimization criteria (opt = tight) in the Gaussian 16[46] implementation of B3PW91[53] with an ultrafine integral grid (int = ultrafine), and Grimme's dispersion correction[54] was employed in all calculations. All structures were fully optimized, and analytical frequency calculations were included on all structures to ensure a zeroth-order (local minimum) or first-order (transition state) saddle point. The minima associated with each transition state were verified by animation of the imaginary frequency. The energy values were calculated at 298 K with the 6-311++G(d,p) basis set[55] for C, H, N, O, S, and K atoms and the SDD basis set with an added f polarization function[52] on rhenium and manganese. The reported energies utilized analytical frequencies, and the zero point corrections from the gas phase optimized geometries and include solvation corrections which were computed using the polarizable continuum model (PCM) method,[56,57] with toluene as the solvent as implemented in Gaussian 16.

General Procedure for Catalytic Reactions. In a typical run, 0.0045 mmol of the catalyst was dissolved in the specific dry solvent, and then the base potassium *tert*-butoxide (0.045 mmol) was added dropwise, followed by the substrate (0.9 mmol). They would all be combined in 20 mL glass vials and transferred into Parr Instrument stainless steel autoclaves under an inert atmosphere. The system would then be purged with H_2 (1 × 20 bar) for 1 min, pressurized with H_2 to the specified pressure, and heated to the specific temperature. The reactions were run in triplicate, and the yields of products were determined by ^{1}H NMR spectroscopy.

■ ASSOCIATED CONTENT

Supporting Information

The Supporting Information is available free of charge at https://pubs.acs.org/doi/10.1021/acs.organomet.2c00261.

Additional X-ray experimental details; ^{1}H, ^{13}C NMR, and 2D spectra; further computational details; pathways; and optimized structures (PDF)

Optimized geometries (XYZ)

Accession Codes

CCDC 2175199−2175201 contain the supplementary crystallographic data for this paper. These data can be obtained free of charge via www.ccdc.cam.ac.uk/data_request/cif, or by emailing data_request@ccdc.cam.ac.uk, or by contacting The Cambridge Crystallographic Data Centre, 12 Union Road, Cambridge CB2 1EZ, UK; fax: +44 1223 336033.

■ AUTHOR INFORMATION

Corresponding Author

Elon A. Ison − *Department of Chemistry, North Carolina State University, Raleigh, North Carolina 27695-8204, United*

https://doi.org/10.1021/acs.organomet.2c00261
Organometallics 2022, 41, 2678−2687

States; orcid.org/0000-0002-2902-2671; Email: eaison@ncsu.edu

Author

Liana Ribeiro Gouveia − *Department of Chemistry, North Carolina State University, Raleigh, North Carolina 27695-8204, United States*

Complete contact information is available at:
https://pubs.acs.org/10.1021/acs.organomet.2c00261

Notes

The authors declare no competing financial interest.

■ ACKNOWLEDGMENTS

We acknowledge the NCSU Office of Information Technology (OIT) High Performance Computing (HPC) for computational support. This work was supported by the National Science Foundation (CHE-2154878). Funding for D8 VENTURE acquisition was provided in part by North Carolina Biotechnology Center grant: NCBC#2019-IDG-1010.

■ REFERENCES

(1) Elsevier, C. J.; de Vries, J. G. *The Handbook of Homogeneous Hydrogenation*; Wiley, 2007.
(2) Arai, N.; Ohkuma, T. Design of Molecular Catalysts for Achievement of High Turnover Number in Homogeneous Hydrogenation. *Chem. Rec.* **2012**, *12*, 284−289.
(3) Balaraman, E.; Gunanathan, C.; Zhang, J.; Shimon, L. J. W.; Milstein, D. Efficient hydrogenation of organic carbonates, carbamates and formates indicates alternative routes to methanol based on CO2 and CO. *Nat. Chem.* **2011**, *3*, 609−614.
(4) Pandey, P.; Dutta, I.; Bera, J. K. Acceptorless Alcohol Dehydrogenation: A Mechanistic Perspective. *Proc. Natl. Acad. Sci., India, Sect. A* **2016**, *86*, 561−579.
(5) Zell, T.; Milstein, D. Hydrogenation and Dehydrogenation Iron Pincer Catalysts Capable of Metal-Ligand Cooperation by Aromatization/Dearomatization. *Acc. Chem. Res.* **2015**, *48*, 1979−1994.
(6) Zou, Y. Q.; Chakraborty, S.; Nerush, A.; Oren, D.; Diskin-Posner, Y.; Ben-David, Y.; Milstein, D. Highly Selective, Efficient Deoxygenative Hydrogenation of Amides Catalyzed by a Manganese Pincer Complex via Metal-Ligand Cooperation. *ACS Catal.* **2018**, *8*, 8014−8019.
(7) Noyori, R.; Sandoval, C. A.; Muñiz, K.; Ohkuma, T. Metal-Ligand Bifunctional Catalysis for Asymmetric Hydrogenation. *Philos. Trans. R. Soc., A* **2005**, *363*, 901−912.
(8) Dub, P. A.; Scott, B. L.; Gordon, J. C. Air-Stable NNS (ENENES) Ligands and Their Well-Defined Ruthenium and Iridium Complexes for Molecular Catalysis. *Organometallics* **2015**, *34*, 4464−4479.
(9) Gunanathan, C.; Milstein, D. Metal-Ligand Cooperation by Aromatization-Dearomatization: A New Paradigm in Bond Activation and "Green" Catalysis. *Acc. Chem. Res.* **2011**, *44*, 588−602.
(10) Kumar, A.; Janes, T.; Espinosa-Jalapa, N. A.; Milstein, D. Manganese Catalyzed Hydrogenation of Organic Carbonates to Methanol and Alcohols. *Angew. Chem., Int. Ed.* **2018**, *57*, 12076−12080.
(11) Balaraman, E.; Gnanaprakasam, B.; Shimon, L. J. W.; Milstein, D. Direct Hydrogenation of Amides to Alcohols and Amines under Mild Conditions. *J. Am. Chem. Soc.* **2010**, *132*, 16756−16758.
(12) Kumar, A.; von Wolff, N.; Rauch, M.; Zou, Y. Q.; Shmul, G.; Ben-David, Y.; Leitus, G.; Avram, L.; Milstein, D. Hydrogenative Depolymerization of Nylons. *J. Am. Chem. Soc.* **2020**, *142*, 14267−14275.
(13) Landwehr, A.; Dudle, B.; Fox, T.; Blacque, O.; Berke, H. Bifunctional Rhenium Complexes for the Catalytic Transfer-Hydrogenation Reactions of Ketones and Imines. *Chem.—Eur. J.* **2012**, *18*, 5701−5714.
(14) Noyori, R.; Ohkuma, T. Asymmetric Catalysis by Architectural and Functional Molecular Engineering: Practical Chemo- and Stereoselective Hydrogenation of Ketones. *Angew. Chem., Int. Ed.* **2001**, *40*, 40−73.
(15) van der Vlugt, J. I. Cooperative Catalysis with First-Row Late Transition Metals. *Eur. J. Inorg. Chem.* **2012**, 363−375.
(16) Buhaibeh, R.; Filippov, O. A.; Bruneau-Voisine, A.; Willot, J.; Duhayon, C.; Valyaev, D. A.; Lugan, N.; Canac, Y.; Sortais, J. B. Phosphine-NHC Manganese Hydrogenation Catalyst Exhibiting a Non-Classical Metal-Ligand Cooperative H 2 Activation Mode. *Angew. Chem., Int. Ed.* **2019**, *58*, 6727−6731.
(17) Ben-Ari, E.; Leitus, G.; Shimon, L. J. W.; Milstein, D. Metal−Ligand Cooperation in C−H and H2 Activation by an Electron-Rich PNP Ir(I) System: Facile Ligand Dearomatization−Aromatization as Key Steps. *J. Am. Chem. Soc.* **2006**, *128*, 15390−15391.
(18) Krall, E. M.; Klein, T. W.; Andersen, R. J.; Nett, D. S.; Glasgow, B. C.; Reader, S. P.; Dauphinais, A. A.; Mc Ilrath, M. J.; Fischer, N. J.; Carney, M. J.; Hudson, D. J.; Robertson, N. J. Controlled Hydrogenative Depolymerization of Polyesters and Polycarbonates Catalyzed by Ruthenium(II) PNN Pincer Complexes. *Chem. Commun.* **2014**, *50*, 4884−4887.
(19) Chen, X.; Jia, W.; Guo, R.; Graham, T. W.; Gullons, M. A.; Abdur-Rashid, K. Highly Active Iridium Catalysts for the Hydrogenation of Ketones and Aldehydes. *Dalton Trans.* **2009**, 1407−1410.
(20) Zhang, J.; Balaraman, E.; Leitus, G.; Milstein, D. Electron-Rich PNP- and PNN-Type Ruthenium(II) Hydrido Borohydride Pincer Complexes. Synthesis, Structure, and Catalytic Dehydrogenation of Alcohols and Hydrogenation of Esters. *Organometallics* **2011**, *30*, 5716−5724.
(21) Kuninobu, Y.; Takai, K. Organic Reactions Catalyzed by Rhenium Carbonyl Complexes. *Chem. Rev.* **2011**, *111*, 1938−1953.
(22) Weber, S.; Stöger, B.; Veiros, L. F.; Kirchner, K. Rethinking Basic Concepts-Hydrogenation of Alkenes Catalyzed by Bench-Stable Alkyl Mn(I) Complexes. *ACS Catal.* **2019**, *9*, 9715−9720.
(23) Wei, D.; Bruneau-Voisine, A.; Chauvin, T.; Dorcet, V.; Roisnel, T.; Valyaev, D. A.; Lugan, N.; Sortais, J. B. Hydrogenation of Carbonyl Derivatives Catalysed by Manganese Complexes Bearing Bidentate Pyridinyl-Phosphine Ligands. *Adv. Synth. Catal.* **2018**, *360*, 676−681.
(24) Fertig, R.; Irrgang, T.; Freitag, F.; Zander, J.; Kempe, R. Manganese-Catalyzed and Base-Switchable Synthesis of Amines or Imines via Borrowing Hydrogen or Dehydrogenative Condensation. *ACS Catal.* **2018**, *8*, 8525−8530.
(25) Zhang, L.; Tang, Y.; Han, Z.; Ding, K. Lutidine-Based Chiral Pincer Manganese Catalysts for Enantioselective Hydrogenation of Ketones. *Angew. Chem., Int. Ed.* **2019**, *58*, 4973−4977.
(26) Ling, F.; Hou, H.; Chen, J.; Nian, S.; Yi, X.; Wang, Z.; Song, Di.; Zhong, W. Highly Enantioselective Synthesis of Chiral Benzhydrols via Manganese Catalyzed Asymmetric Hydrogenation of Unsymmetrical Benzophenones Using an Imidazole-Based Chiral PNN Tridentate Ligand. *Org. Lett.* **2019**, *21*, 3937−3941.
(27) Yang, W.; Chernyshov, I. Y.; van Schendel, R. K. A.; Weber, M.; Müller, C.; Filonenko, G. A.; Pidko, E. A. Robust and Efficient Hydrogenation of Carbonyl Compounds Catalysed by Mixed Donor Mn(I) Pincer Complexes. *Nat. Commun.* **2021**, *12*, 12.
(28) Valyaev, D. A.; Lavigne, G.; Lugan, N. Manganese Organometallic Compounds in Homogeneous Catalysis: Past, Present, and Prospects. *Coord. Chem. Rev.* **2016**, *308*, 191−235.
(29) Kallmeier, F.; Kempe, R. Manganese Complexes for (De)-Hydrogenation Catalysis: A Comparison to Cobalt and Iron Catalysts. *Angew. Chem., Int. Ed.* **2018**, *57*, 46−60.
(30) Freitag, F.; Irrgang, T.; Kempe, R. Mechanistic Studies of Hydride Transfer to Imines from a Highly Active and Chemoselective Manganate Catalyst. *J. Am. Chem. Soc.* **2019**, *141*, 11677−11685.
(31) Elangovan, S.; Garbe, M.; Jiao, H.; Spannenberg, A.; Junge, K.; Beller, M. Hydrogenation of Esters to Alcohols Catalyzed by Defined Manganese Pincer Complexes. *Angew. Chem., Int. Ed.* **2016**, *55*, 15364−15368.
(32) Glatz, M.; Stöger, B.; Himmelbauer, D.; Veiros, L. F.; Kirchner, K. Chemoselective Hydrogenation of Aldehydes under Mild, Base-Free Conditions: Manganese Outperforms Rhenium. *ACS Catal.* **2018**, *8*, 4009−4016.

(33) Kaithal, A.; Hölscher, M.; Leitner, W. Catalytic Hydrogenation of Cyclic Carbonates Using Manganese Complexes. *Angew. Chem., Int. Ed.* **2018**, *57*, 13449−13453.
(34) Papa, V.; Cabrero-Antonino, J. R.; Alberico, E.; Spanneberg, A.; Junge, K.; Junge, H.; Beller, M. Efficient and Selective Hydrogenation of Amides to Alcohols and Amines Using a Well-Defined Manganese-PNN Pincer Complex. *Chem. Sci.* **2017**, *8*, 3576−3585.
(35) Weber, S.; Brünig, J.; Veiros, L. F.; Kirchner, K. Manganese-Catalyzed Hydrogenation of Ketones under Mild and Base-Free Conditions. *Organometallics* **2021**, *40*, 1388−1394.
(36) Das, K.; Mondal, A.; Pal, D.; Srivastava, H. K.; Srimani, D. Phosphine-Free Well-Defined Mn(I) Complex-Catalyzed Synthesis of Amine, Imine, and 2,3-Dihydro-1H-perimidine via Hydrogen Auto-transfer or Acceptorless Dehydrogenative Coupling of Amine and Alcohol. *Organometallics* **2019**, *38*, 1815−1825.
(37) Filonenko, G. A.; van Putten, R.; Hensen, E. J. M.; Pidko, E. A. Catalytic (de)hydrogenation promoted by non-precious metals - Co, Fe and Mn: recent advances in an emerging field. *Chem. Soc. Rev.* **2018**, *47*, 1459−1483.
(38) Werkmeister, S.; Neumann, J.; Junge, K.; Beller, M. Pincer-Type Complexes for Catalytic (De)Hydrogenation and Transfer (De)-Hydrogenation Reactions: Recent Progress. *Chem.—Eur. J.* **2015**, *21*, 12226−12250.
(39) Chandra, P.; Ghosh, T.; Choudhary, N.; Mohammad, A.; Mobin, S. M. Recent Advancement in Oxidation or Acceptorless Dehydrogenation of Alcohols to Valorised Products Using Manganese Based Catalysts. *Coord. Chem. Rev.* **2020**, *411*, 213241.
(40) Carney, J. R.; Dillon, B. R.; Thomas, S. P. Recent Advances of Manganese Catalysis for Organic Synthesis. *Eur. J. Org. Chem.* **2016**, *2016*, 3912−3929.
(41) Snider, B. B. Manganese(III)-Based Oxidative Free-Radical Cyclizations. *Chem. Rev.* **1996**, *96*, 339−364.
(42) Espinosa-Jalapa, N. A.; Nerush, A.; Shimon, L. J. W.; Leitus, G.; Avram, L.; Ben-David, Y.; Milstein, D. Manganese-Catalyzed Hydrogenation of Esters to Alcohols. *Chem.—Eur. J.* **2017**, *23*, 5934−5938.
(43) Garduño, J. A.; García, J. J. Non-Pincer Mn(I) Organometallics for the Selective Catalytic Hydrogenation of Nitriles to Primary Amines. *ACS Catal.* **2019**, *9*, 392−401.
(44) Choualeb, A.; Lough, A. J.; Gusev, D. G. Hydridic Rhenium Nitrosyl Complexes with Pincer-Type PNP Ligands. *Organometallics* **2007**, *26*, 3509−3515.
(45) Li, H.; Wei, D.; Bruneau-Voisine, A.; Ducamp, M.; Henrion, M.; Roisnel, T.; Dorcet, V.; Darcel, C.; Carpentier, J. F.; Soulé, J. F.; Sortais, J. B. Rhenium and Manganese Complexes Bearing Amino-Bis-(Phosphinite) Ligands: Synthesis, Characterization, and Catalytic Activity in Hydrogenation of Ketones. *Organometallics* **2018**, *37*, 1271−1279.
(46) Frisch, M. J.; Trucks, G. W.; Schlegel, H. B.; Scuseria, G. E.; Robb, M. A.; Cheeseman, J. A.; Scalmani, G.; Barone, V.; Petersson, G. A.; Nakatsuji, H.; Li, X.; Caricato, M.; Marenich, A.; Bloino, J.; Janesko, B. G.; Gomperts, R.; Mennucci, B.; Hratchian, H. P.; Ortiz, J. V.; Izmaylov, A. F.; Sonnenberg, J. L.; Williams-Young, D.; Ding, F.; Lipparini, F.; Egidi, F.; Goings, J.; Peng, B.; Petrone, A.; Henderson, T.; Ranasinghe, D.; Zakrzewski, V. G.; Gao, J.; Rega, N.; Zheng, G.; Liang, W.; Hada, M.; Ehara, M.; Toyota, K.; Fukuda, R.; Hasegawa, J.; Ishida, M.; Nakajima, T.; Honda, Y.; Kitao, O.; Nakai, H.; Vreven, T.; Throssell, K.; Montgomery, J. A., Jr; Peralta, J. E.; Ogliaro, F.; Bearpark, M.; Heyd, J. J.; Brothers, E.; Kudin, K. N.; Staroverov, V. N.; Keith, T.; Kobayashi, R.; Normand, J.; Raghavachari, K.; Rendell, A.; Burant, J. C.; Iyengar, S. S.; Tomasi, J.; Cossi, M.; Millam, J. M.; Klene, M.; Adamo, C.; Cammi, R.; Ochterski, J. W.; Martin, R. L.; Morokuma, K.; Farkas, O.; Foresman, J. B.; Fox, D. J. *Gaussian 16*, Revision A.03; Gaussian, Inc.: Wallingford CT, 2016.
(47) Rassolov, V. A.; Ratner, M. A.; Pople, J. A.; Redfern, P. C.; Curtiss, L. A. 6-31G* Basis Set for Third-Row Atoms. *J. Comput. Chem.* **2001**, *22*, 976−984.
(48) Rassolov, V. A.; Pople, J. A.; Ratner, M. A.; Windus, T. L. 6-31G* Basis Set for Atoms K through Zn. *J. Chem. Phys.* **1998**, *109*, 1223−1229.
(49) Dolg, M.; Stoll, H.; Preuss, H.; Pitzer, R. M. Relativistic and Correlation Effects for Element 105 (Hahnium, Ha). A Comparative Study of M and MO (M = Nb, Ta, Ha) Using Energy-Adjusted Ab Initio Pseudopotentials. *J. Phys. Chem.* **1993**, *97*, 5852.
(50) Andrae, D.; Häußermann, U.; Dolg, M.; Stoll, H.; Preuß, H. Energy-adjustedab initio pseudopotentials for the second and third row transition elements. *Theor. Chim. Acta* **1990**, *77*, 123−141.
(51) Kaupp, M.; Schleyer, P. V. R.; Stoll, H.; Preuss, H. Pseudopotential approaches to Ca, Sr, and Ba hydrides. Why are some alkaline earth MX2compounds bent? *J. Chem. Phys.* **1991**, *94*, 1360−1366.
(52) Ehlers, A. W.; Böhme, M.; Dapprich, S.; Gobbi, A.; Höllwarth, A.; Jonas, V.; Köhler, K. F.; Stegmann, R.; Veldkamp, A.; Frenking, G. A set of f-polarization functions for pseudo-potential basis sets of the transition metals Sc—Cu, Y—Ag and La—Au. *Chem. Phys. Lett.* **1993**, *208*, 111−114.
(53) Perdew, J. P.; Burke, K.; Wang, Y. Generalized Gradient Approximation for the Exchange-Correlation Hole of a Many-Electron System. *Phys. Rev. B: Condens. Matter Mater. Phys.* **1996**, *54*, 16533−16539.
(54) Grimme, S.; Antony, J.; Ehrlich, S.; Krieg, H. A Consistent and Accurate Ab Initio Parametrization of Density Functional Dispersion Correction (DFT-D) for the 94 Elements H-Pu. *J. Chem. Phys.* **2010**, *132*, 154104.
(55) Francl, M. M.; Pietro, W. J.; Hehre, W. J.; Binkley, J. S.; Gordon, M. S.; DeFrees, D. J.; Pople, J. A. Self-consistent molecular orbital methods. XXIII. A polarization-type basis set for second-row elements. *J. Chem. Phys.* **1982**, *77*, 3654−3665.
(56) Cancès, E.; Mennucci, B.; Tomasi, J. A New Integral Equation Formalism for the Polarizable Continuum Model: Theoretical Background and Applications to Isotropic and Anisotropic Dielectrics. *J. Chem. Phys.* **1997**, *107*, 3032−3041.
(57) Mennucci, B.; Tomasi, J. Continuum solvation models: A new approach to the problem of solute's charge distribution and cavity boundaries. *J. Chem. Phys.* **1997**, *106*, 5151−5158.

https://doi.org/10.1021/acs.organomet.2c00261
Organometallics 2022, 41, 2678−2687